ELSEVIER

Contents lists available at ScienceDirect

# Journal of Power Sources

journal homepage: www.elsevier.com/locate/jpowsour





# Metallically conductive $TiB_2$ as a multi-functional separator modifier for improved lithium sulfur batteries

Liming Jin  $^{a,b,c,d}$ , Jie Ni  $^b$ , Chao Shen  $^{c,d}$ , Fenglai Peng  $^g$ , Qiang Wu  $^{c,d}$ , Donghao Ye  $^{c,d}$ , Junsheng Zheng  $^{b,*}$ , Gaoran Li  $^{e,**}$ , Cunman Zhang  $^b$ , Zhoupeng Li  $^{a,f,***}$ , Jim P. Zheng  $^{b,c,d}$ 

- <sup>a</sup> Department of Chemical and Biological Engineering, Zhejiang University, Hangzhou, 310027, China
- b Clean Energy Automotive Engineering Center and School of Automotive Studies, Tongji University, Shanghai, 201804, China
- <sup>c</sup> Aero-Propulsion, Mechatronics and Energy Center, Florida State University, FL, 32310, USA
- d Department of Electrical and Computer Engineering, Florida A&M University-Florida State University College of Engineering, FL, 32310, USA
- e Department of Chemical Engineering, University Waterloo, Waterloo, Ontario, N2L 3G1, Canada
- f Ningbo Research Institute, Zhejiang University, Ningbo, 315100, China
- g Shanghai Motor Vehicle Inspection Certification & Tech Innovation Center Co., Ltd, Shanghai, 201805, China

#### HIGHLIGHTS

- A metallically conductive TiB<sub>2</sub> is developed to modify the separator.
- The TiB2@G separator fulfills strong sulfur immobilization.
- The TiB2@G separator enables a high-efficiency sulfur reutilization.
- A lithium sulfur battery with improved performance is achieved.

# ARTICLE INFO

Keywords:  $TiB_2$  High conductivity Multi-functional separator Lithium sulfur battery

# ABSTRACT

A metallically conductive  $TiB_2$  is developed to construct multifunctional separator toward improved lithium-sulfur (Li–S) battery performance. Coupled with two-dimensional graphene, the obtained  $TiB_2@G$  separator fulfills a synergistic combination of strong physical and chemical sulfur immobilization as well as a high-efficiency sulfur reutilization, thus establishing a robust barrier against the polysulfide shuttling and enabling a fast and durable sulfur electrochemistry. As a result, cells based on  $TiB_2@G$  separator exhibit a high sulfur utilization with 1350 mA h g<sup>-1</sup> capacity at 0.05C, superb rate capability up to 5.0C, and excellent cyclability with a high capacity retention over 85% after 300 cycles at 0.5C. Moreover, significantly mitigated self-discharge and considerably high areal capacity of 5.8 mA h cm<sup>-2</sup> can be also achieved, indicating the great promise of this separator design for the development of high-performance Li–S batteries.

#### 1. Introduction

Lithium sulfur (Li–S) batteries are considered as one of the most promising next-generation battery technologies for future energy storage applications, such as electric vehicles and hybrid electric vehicles, due to their high theoretical energy density (2500 Wh kg<sup>-1</sup>), low cost and good environmental benignity [1–4]. However, there are several challenges need to be well addressed before the practical application of Li–S batteries, including low sulfur utilization, severe volume change

during cycling, and poor sulfur electrochemical reversibility induced by the so-called "shuttle effect". The shuttle effect refers to the situation where the soluble long-chain lithium polysulfides (LiPSs) generated in cathode diffuse to anode to be reduced to form short-chain LiPSs by lithium, which subsequently migrate back to cathode to be recovered into long-chain LiPSs. This continuous migration of LiPSs back and forth accompanied by the chemical/electrochemical redox at both electrodes continuously consume the active materials and result in low coulombic efficiency and poor cycling stability. Hence, the effective suppression of

<sup>\*</sup> Corresponding author.;

<sup>\*\*</sup> Corresponding author.

<sup>\*\*\*</sup> Corresponding author. Department of Chemical and Biological Engineering, Zhejiang University, Hangzhou, 310027, China E-mail addresses: jszheng@tongji.edu.cn, jzheng2@fsu.edu (J. Zheng), lgr19890725@gmail.com (G. Li), zhoupengli@zju.edu.cn (Z. Li).

shuttle effect has become an essential and everlasting topic in Li–S research field [5].

In the past few decades, a great number of studies has been implemented for suppressing the shuttle effect in Li–S batteries. These multifarious strategies can be basically classified into three categories: (i) restraining the LiPSs dissolution by various physical and/or chemical adsorbents, including carbonaceous materials [6–8], metal oxide [9–12], metal nitride [13], etc. in cathode; (ii) utilizing specific electrolyte additives such as LiNO<sub>3</sub> [14], LiPSs [15], La(NO<sub>3</sub>)<sub>3</sub> [16], etc., to build surface protection for cathode and/or anode to suppress the detrimental reactions by LiPSs shuttling; (iii) constructing functional separator to block the migration and simultaneously favor the reutilization of the dissolved LiPSs [17–19].

Among them, separator modification with facile fabrication, good manipulability, and considerable validity, have shown particular advantages for the improvement of Li-S battery performance [20,21]. Up to now, several scenarios of functional separators have been proposed. Carbonaceous materials, such as carbon quantum/nano-dot (zero dimension) [22,23], carbon nanotube/fiber (one dimension) [24,25], graphene (two dimension) [26,27], porous carbon (three dimension) [28], etc., have been extensively studied to functionalize the conventional polypropylene separator to suppress the LiPSs shuttling. Carbon-modified separators have shown certain efficacy in adsorbing and blocking LiPSs. However, the weak interactions between carbonaceous materials and LiPSs fail to efficiently immobilize the sulfur species. Under such circumstance, polar materials are attracting increasing research enthusiasm to impose the stronger chemical sulfur confinement for inhibiting LiPSs shuttling. The chemical interactions between polar agents and LiPSs have been demonstrated with intensified sulfur immobilization thus leading to considerable improvement of sulfur reaction reversibility [29-33]. Even so, the adsorbed LiPSs are found difficult to be efficiently reutilized ascribed to the non/poor conductive nature of common polar agents such as metal oxides [34], let alone the even severer challenge of shuttle inhibition under long-term cycling and/or high sulfur loading conditions, which give rise to the limited sulfur utilization and poor reaction kinetics [35]. Therefore, the development of advanced separator material that combines high conductivity and strong LiPSs absorbability is crucial yet still challenging for the enhancement of Li-S battery performance.

Herein, we developed a metallically conductive TiB2 as multifunctional modifier to construct highly effective TiB2@G separators for improved Li–S batteries. Graphene was employed as the film-forming agent to enable a facile fabrication of TiB2-based separator by suction filtration, which simultaneously establishes a considerable physical obstruction for LiPSs migration as well as a facilitated long-range electron conduction for sulfur electrochemical reductions. The as-developed TiB<sub>2</sub> delivers a high conductivity up to  $\sim 10^5$  S/cm, which is close to metal level and 14-15 order of magnitude higher than those of the commonly used metal oxides and sulfides [36]. Moreover, the polar nature endows TiB<sub>2</sub> with a strong chemical interaction with LiPSs via the Ti-S and B-S bonds, thus contributing to the high-efficiency adsorption and reutilization of LiPS, as well as the resultant expedite and stable electrochemical performance. As such, the  $TiB_2@G$  separator enables a high capacity of  $1350\,\mathrm{mA}\,\mathrm{h}~\mathrm{g}^{-1}$  at 0.05C, a high-rate capability of 700 mA h  $g^{-1}$  at 5.0C, and excellent cyclability with 850 mA h  $g^{-1}$  capacity retained after 300 cycles at 0.5C. Beyond that, this TiB2@G design also suppresses the self-discharge behaviors and enhances the high-loading performance with a high areal capacity of 5.8 mA h cm<sup>-2</sup> under a sulfur loading up to 4.5 mg cm<sup>-2</sup>. These results strongly demonstrate the great promise of TiB2@G separator in development of high-performance Li-S batteries.

#### 2. Materials characterizations

## 2.1. Preparation of TiB2 particles

 $TiB_2$  particles were prepared by a simple and low-cost two-step ball-milling approach [37]. In brief, the Titanium dioxide (Aladdin, particle size:  $0.2\text{--}0.4\,\mu\text{m}$ ) was mixed with Boric oxide (Aladdin, 99.99% metal basis) and magnesium (Aladdin), and the mixtures were sealed in ball-mills with the speed of 400 rpm for 96 h. After that,  $TiB_2$  particles were obtained by leaching the milled product with  $1.0\,\text{M}$  HCl for 5 h to remove magnesium oxide.

## 2.2. Preparation of TiB2@G separator

The graphene is prepared by ball-milling method as reported in our previous paper [39]. TiB<sub>2</sub> particles (10.0 mg) and graphene (10.0 mg) were firstly mixed in 10.0 mL ethyl alcohol. The mixture was ultrasonicated for 30 min and rested for 10 min, which was repeated three times. The obtained homogeneous mixture was filtrated with Celgard 2400 separator as filter membrane. After drying at 80 °C overnight, the TiB<sub>2</sub>@G separator was obtained. For comparison, the sole graphene-based separator was also prepared through the process but without TiB<sub>2</sub>. The area of separator for coin cells is 1.98 cm<sup>2</sup>, and the loadings of TiB<sub>2</sub>@G and G on the separators are 1.75 mg and 3.50 mg, respectively.

## 2.3. Preparation of LiPSs

 $Li_2S$  (46.0 mg) and S (224.0 mg) were mixed and dissolved into Tetrahydrofuran (THF) inside an Ar-filled glovebox (H<sub>2</sub>O, O<sub>2</sub> < 0.1 ppm). The mixture was stirred at 30 °C overnight to form 0.08 M Li<sub>2</sub>S<sub>8</sub> (THF) solution [6,16].

# 2.4. Material characterizations

The morphologies of materials were observed through field emission scanning electron microscopy (FESEM, Zeiss Ultra55) at 5 kV, and transmission electron microscopy (TEM, Hitachi H-9500) at 300 kV. The element states were investigated by X-ray photoemission spectroscopy (XPS) using a PHI–5000C ESCA system (PerkinElmer) with Mg K $\alpha$  radiation (h $\nu$  = 1253.6 ev). The material structures were measured by X-ray diffraction (XRD) with Cu K $\alpha$  radiation ( $\lambda$  = 1.5406 Å), (X'Pert PRO PANalytical B.V.)

#### 2.5. Electrochemical evaluations

Sulfur/super P composite (S/SP) electrodes were prepared using doctor-blade method. The mixture of sulfur (50 wt%), super P (35 wt%) and PVDF (15 wt%) was dispersed into N-methyl-2-pyrrolidone (NMP) solvent for electrode preparation. After coating the slurry onto Al foil, the electrode was dried in room temperature overnight followed by vacuum drying at 80 °C for 12 h. The electrode was punched into wafer with the dimeter of 12 mm for coin cell preparation. Sulfur loading was controlled at  $1.5\,\mathrm{mg\,cm^{-2}}$  or  $4.5\,\mathrm{mg\,cm^{-2}}$ . Coin cells (CR2032) were fabricated in Ar-filled glove box with the prepared S/SP electrode as cathode, lithium foil as counter electrode and prepared multi-functional membrane as separator. The electrolyte consists of lithiumbis trifluoromethane sulfonimide (LiTFSI, 1.0 M) and LiNO<sub>3</sub> (0.1 M) in DME-DOL solution (1:1 in volume ratio), and the electrolyte amount for the coin cell is controlled to an electrolyte and sulfur ratio of 30  $\mu$ L/mg<sub>sulfur</sub>. Galvanostatic charge and discharge tests were conducted within 1.8–2.6 V (vs. Li/Li $^{+}$ ) at 25 °C.

## 3. Results and discussion

TiB<sub>2</sub> particles were prepared by a simple and low-cost ball-milling

approach coupled with HCl leaching process [37]. Fig. 1a and Fig. S1 show the morphologies of the obtained  $TiB_2$  under FESEM, which are mainly particles with an average size of  $1.0\,\mu m$ . The XRD pattern (Fig. 1b) confirms the successful preparation of highly crystalline  $TiB_2$  by showing a group of clear and sharp peaks of  $TiB_2$  (JCPDS PDF#35-0741), corresponding to the (001), (100), (101), (002), (110), (111), and (201) planes of hexagonal  $TiB_2$ , respectively [36]. Moreover, XPS was performed to illustrate the elemental status of as-prepared  $TiB_2$ . Fig. 1e shows two predominant Ti 2p<sub>3/2</sub> components, which correspond to Ti-B bond at 454.1eV, Ti-O bond at 458.5 eV, and one Ti 2p<sub>1/2</sub> component at 464.3 eV. The Ti-O bond is an avoidable particle oxidation when the  $TiB_2$  particles are exposed to air. On the other hand, the Ti-B and B-O bonds at 187.3 eV and 191.9 eV are also detected (Fig. 1f), which are consistent with the previous reports [36].

To demonstrate the physical and/or chemical interactions between graphene and TiB<sub>2</sub> with LiPSs, the TiB<sub>2</sub> particles, graphene, graphene/ TiB<sub>2</sub> composites were immersed in Li<sub>2</sub>S<sub>8</sub> solution for 2 h, respectively. As shown in Fig. 1c, the original Li<sub>2</sub>S<sub>8</sub> solution shows a dark-brown color, which turns into light-brown color after TiB2 immersion, light-yellow color after graphene adsorption, and totally clear after graphene/TiB<sub>2</sub> interaction respectively, indicating their great absorbability to Li<sub>2</sub>S<sub>8</sub> by physical and/or chemical interactions respectively. XPS analysis was performed to verify the chemical interactions between TiB2 and Li2S8. The pure Li<sub>2</sub>S<sub>8</sub> shows two pairs of peaks in S 2p spectrum (Fig. 1d) corresponding to the typical S<sub>T</sub> and S<sub>B</sub> peaks, and the S<sub>T</sub> 2p 1/2 bond and  $S_B 2p 1/2$  are settled at (161.0 eV) and  $S_B bond (162.5 eV) [6,8,9,16]$ . By contrast, the S 2p spectrum of Li<sub>2</sub>S<sub>8</sub> adsorbed on TiB<sub>2</sub> shifts to a higher binding energy range due to the strong chemical interactions between S and TiB<sub>2</sub>, which is similarly reported in literatures [38]. For another, the Ti 2p and B 1s spectrums are shifted to lower binding energies as shown in Fig. 1e–f, since the sulfur in  $\text{Li}_2S_8$  bears the negative charge, once it contact with TiB2, the electron is donated to the Ti and B atoms simultaneously, which has been demonstrated in other metal boride. These results illustrate the strong double chemical interactions by S–Ti and S–B bond. Therefore, TiB2 is expected as a desirable LiPSs adsorbent on separator to immobilize the active sulfur by strong chemical interactions between TiB<sub>2</sub> and LiPSs for improved Li–S electrochemical performance. Therefore, the metallically conductive TiB2 particles with a high

conductivity up to  $\sim 10^5$  S/cm were coupled with graphene as a novel separator (TiB2@G) through suction filtration as shown in Fig. 2a. By comparison, the obtained TiB2@G separator well blocks the pores on pristine Celgard membrane surface due to the spreading of 2D structured graphene substrate, which is capable of physically suppress the migration of LiPSs across the separator (Fig. 2b-c). Fig. 2d-e show the highresolution FESEM images of the Celgard and TiB2@G layer surface, in which the TiB<sub>2</sub> particles can be observed uniformly dispersed in graphene base. The cross-section images of TiB2@G (Fig. 2g) and G separator (Fig. 2f) confirm the tight coating of the functional layers with an average thickness of  $12.75\,\mu m$  and  $12.05\,\mu m$ , respectively. The  $N_2$ adsorption-desorption isotherms measurements were carried out to evaluate the specific surface area (SSA) of TiB2@G separator and G separator. The TiB2@G separator and G separator both display high SSA, i.e.  $235.7 \,\mathrm{m}^2\,\mathrm{g}^{-1}$  and  $507.5 \,\mathrm{m}^2\,\mathrm{g}^{-1}$  as shown in Fig. S2, which enables to adsorb the LiPSs by physical interactions. Therefore, the TiB2@G separators expected to physically and chemically adsorb LiPSs simultaneously and efficiently inhibit the shuttle effect when implemented as separator in Li-S configuration.

In order to evaluate the practical effect of the as-developed TiB<sub>2</sub>@G separator on battery performance, coin cells were assembled with S/SP composites as cathode, lithium foil as anode, and different separators. As shown in Fig. 3a-b and Fig. S3, the TiB2@G separator enables a high initial specific capacity of 1350 mA h  $g^{-1}$  at 0.05C (1C = 1675 mA  $g^{-1}$ ) with two clear discharge plateaus at 2.3 V and 2.1 V, which correspond to the two-step sulfur reduction from element sulfur to soluble LiPSs and subsequently into Li<sub>2</sub>S/Li<sub>2</sub>S<sub>2</sub>, respectively [6,16]. After 50 cycles at 0.2C, a high specific capacity of  $1050 \,\mathrm{mAhg}^{-1}$  can be well maintained by the TiB2@G separator, indicating its good cycling stability. By contrast, G-based and pristine Celgard separators deliver much lower initial capacity of 960 mA h g<sup>-1</sup> and 900 mA h g<sup>-1</sup> at 0.05C, respectively, with poorer capacity retention of 805 mAh g<sup>-1</sup> (for G) and 780 mA h g<sup>-1</sup> (for Celgard) after 50 cycles (Fig. 3a-b and Fig. S4). The high capacity and cyclability of cells with TiB2@G separator originate from the physical barrier and chemical LiPSs adsorption established by the TiB<sub>2</sub>@G separator, which efficiently suppress the shuttle effect and facilitate the reutilization of the dissolved LiPS, thus leading to enhanced sulfur utilization and electrochemical reversibility. Such effect

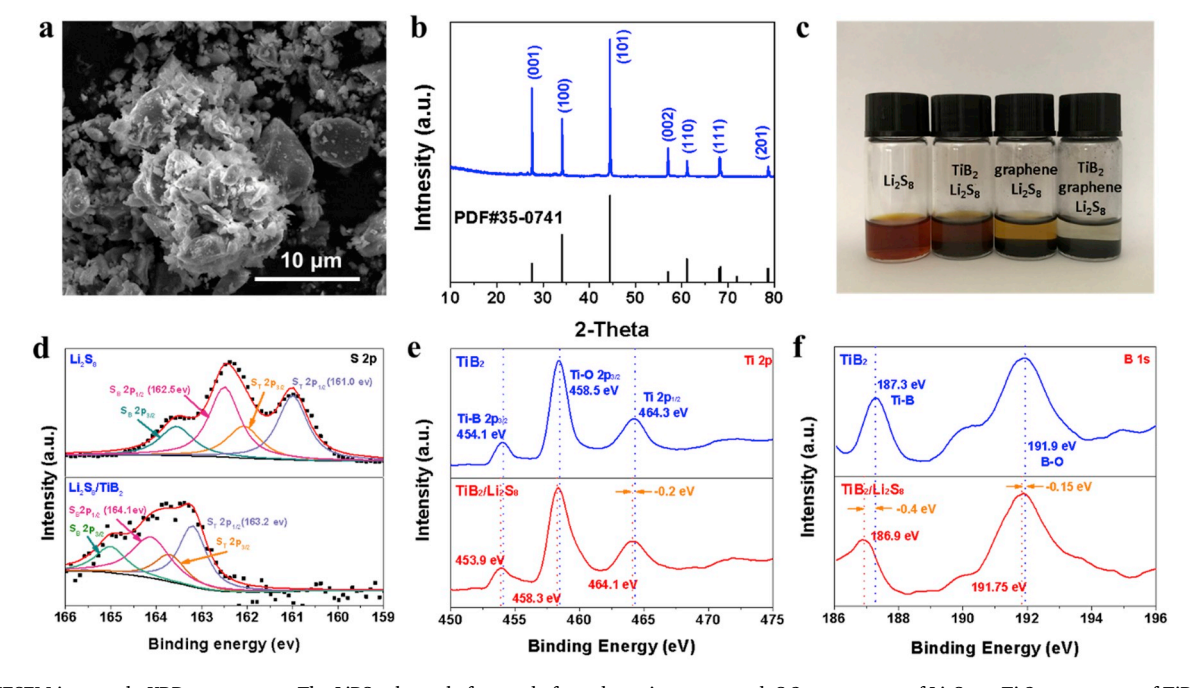


Fig. 1. a. FESEM images; b. XRD spectrum; c. The LiPSs photos before and after adsorption process; d. S 2p spectrums of  $Li_2S_8$ ; e. Ti 2p spectrums of  $TiB_2$  and f. B 1s spectrums of  $TiB_2$  before and after adsorption.

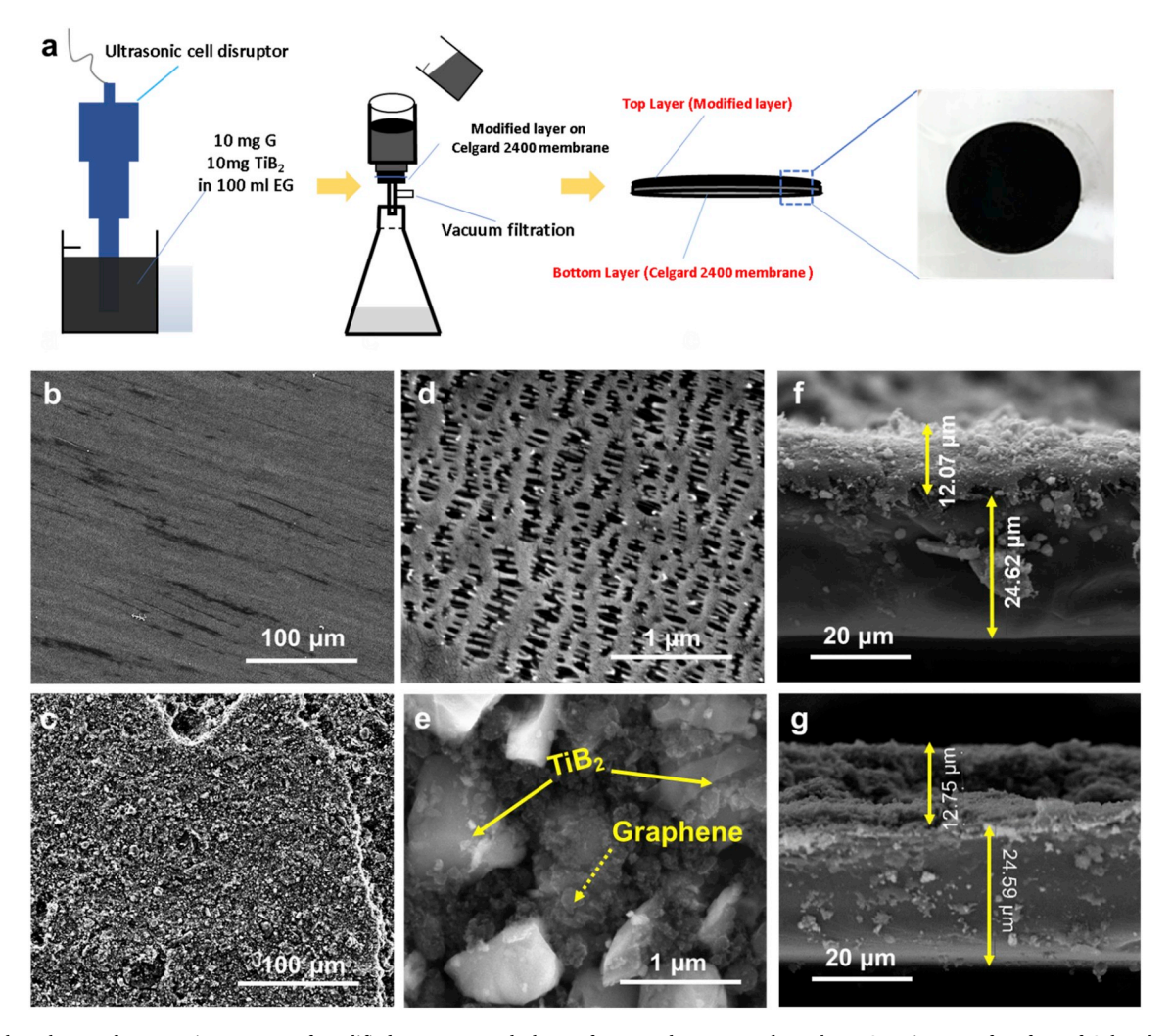


Fig. 2. a. The scheme of preparation process of modified separator and photo of prepared separator; b-c. The FESEM images of surface of Celgard and TiB<sub>2</sub>@G separator; d-e. High resolution FESEM images of Celgard and TiB<sub>2</sub>@G; The cross-section FESM images of (f) G and (g) TiB<sub>2</sub>@G.

can be further confirmed by the ratio of lower-plateau capacity to upper-plateau capacity ( $Q_L/Q_U$ ) in discharge profile, which is a well-recognized indicator of sulfur redox reversibility (Fig. S3) [23]. As shown in Fig. 3c and Fig. S5, TiB<sub>2</sub>@G delivers a persistently higher  $Q_U$ , while its  $Q_L/Q_U$  ratio also maintains the highest among different separators upon 50 cycles, indicating that soluble the LiPSs generated in the initial discharge stage can be more efficiently utilized to form insoluble Li<sub>2</sub>S<sub>2</sub>/Li<sub>2</sub>S, as well as the resultant enhanced electrochemical reversibility attributed to the great superiorities of TiB<sub>2</sub>@G separator.

Apart from that, the highly conductive nature of TiB2 and its strong interactions with LiPSs are also expected to accelerate sulfur electrochemical reaction kinetics [38]. Fig. 3a displays the charge-discharge profiles of cells with TiB2@G, G and Celgard separators. It can be noted that the TiB<sub>2</sub>@G enables an obviously smaller potential gap than that of other samples, indicating its smaller electrochemical polarization and faster sulfur reaction kinetics. This kinetics improvement can be further confirmed by the multi-rate cycling comparison from 0.2C to 5.0C as shown in Fig. 3d-e. The TiB2@G cell delivers an initial capacity of 1200 mA h  $g^{-1}$  at 0.2C and maintains 700 mA h  $g^{-1}$  even a high rate up to 5.0C (corresponding to  $\sim$ 60% capacity retention), which recovers to 1000 mA h g<sup>-1</sup> when reducing the C-rate back to 0.2C, indicating its excellent rate capability and high electrochemical reversibility. By contrast, G and Celgard separator exhibit much poorer rate performance with a lower capacity of 422 and 272 mA h  $g^{-1}$  at 5.0C, respectively, as well as much severer degradation in voltage profiles (Fig. S6). Fig. 3f shows the potential gap comparisons at various C rates, which reveals

TiB<sub>2</sub>@G with the lowest potential gap among them also indicating its best reaction kinetic behaviors. Furthermore, long-term cycling evaluation was conducted at 0.5C to investigate the cell cyclability with different separators. As shown in Fig. 3g, the TiB2@G cell exhibits a high initial capacity of 1000 mAhg<sup>-1</sup> and a high capacity retention of 850 mA h g<sup>-1</sup> after 300 cycles with a minimum capacity fading rate of 0.05% per cycle, which is much lower than that with G (0.09%) and Celgard (0.25%) separators, demonstrating its outstanding cycling stability. All these results strongly manifest the great validity of TiB2@G separator in boosting the sulfur utilization and stabilizing the sulfur redox reactions to achieve fast and stable sulfur electrochemistry, which are originated from the multi-functions of TiB2@G separator, including (1) restraining the LiPSs shuttle by physical (two dimensional graphene) and chemical interactions (Ti-S and B-S interactions), which enables a higher specific capacity; (2) reutilizing the adsorbed LiPSs more efficiently due to the high conductivity of TiB2, which exhibits great effectiveness in improving the Li-S battery performance.

To further investigate the functions of  $TiB_2@G$  in suppressing the shuttling of LiPSs, the surface morphologies of lithium foil after cycling were examined by FESEM as shown in Fig. 4a–c. In comparison with fresh lithium foil (Fig. S7), much more rough surface can be observed due to the detrimental reactions between the shuttled LiPSs and metallic lithium [8,38]. It is worth noting that the lithium anode disassembled from the  $TiB_2@G$ -based cell shows a much smoother surface than those with other separators, suggesting the significant suppression of the shuttle effect by the  $TiB_2@G$  separator. This result can be further

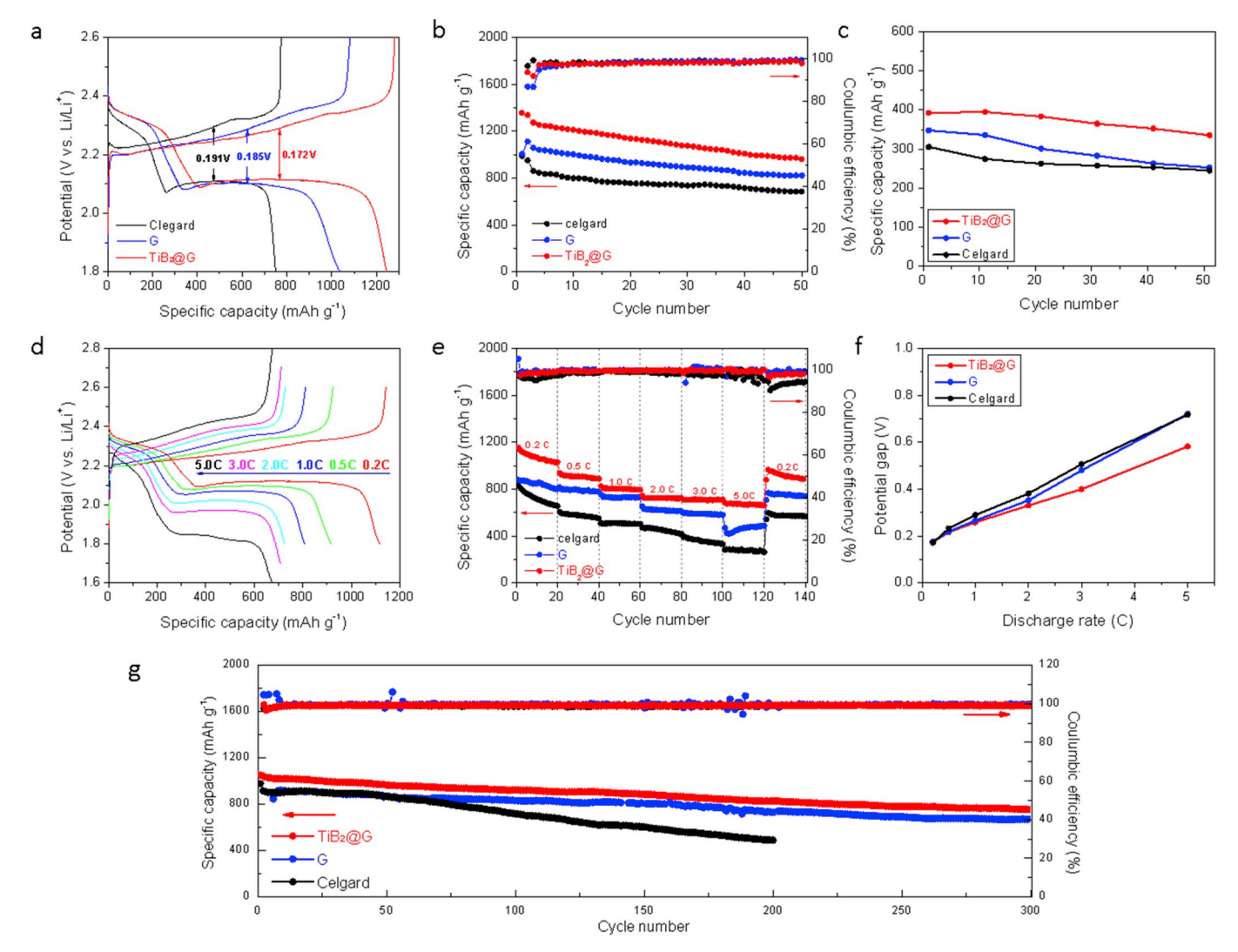


Fig. 3. a. The charge and discharge profiles comparison; b. The cycling performance at 0.2C (first two cycles at 0.05C) comparisons; c. The upper plateau discharge capacity comparisons; d. Multi-rate charge and discharge profiles of  $TiB_2@G$ ; e. Multi-rate performance comparisons; f. The potential gap comparisons; g. Long-term cycling performance comparisons of  $TiB_2@G$ , G and Celgard.

illustrated by EIS evaluation before and after cycling. At fresh state, the EIS curves consist of a semi-circle at high frequency area and a slope at a low frequency area, corresponding to the charge transfer (Rct) and ionic diffusion resistances, respectively (Fig. 4d), while the intercept with X-axis at high frequency represents the ohmic resistance (Ro) [39-42]. Apparently, the TiB2@G separator fulfills a smaller Rct than pristine Celgard separator benefiting from its high conductivity, but a slightly higher Rct than G-based separator probably ascribed to the relatively thicker coating layer. After cycling, the EIS curves are composed of two semi-circles and a slope line (Fig. 4e). The additional semi-circle refers to the charge transfer within the resistive SEI layer on lithium surface, which is highly subject to the amount of LiPSs and their reaction extent with metallic lithium. The EIS patterns were fitted according to the equivalent circuit as shown in Fig. S8, while the obtained resistance were compared in Fig. 4f [35]. It can be perceived that the TiB2@G delivers the smallest Ro and Rct, which contribute to the fast reaction kinetics in the according cells. More importantly, TiB<sub>2</sub>@G separator also achieves the smallest interfacial charge transfer resistance on Li surface after cycling, further indicating its great capability of decreasing the detrimental reactions between LiPSs and lithium anode as well as resultantly inhibiting the polysulfide shuttling behaviors.

Based on the above results, the practical potential of TiB<sub>2</sub>@G was further explored by self-charging and high-loading performance

evaluations. As for the self-discharging test, cells were firstly cycled 20 times at 0.2C (first two cycles at 0.05C) and followed by resting for 48 h to record the voltage variation (Fig. 5a-b). During the rest process, the TiB<sub>2</sub>@G cell shows a high and stable open circuit voltage (OCV) profile with a high voltage retention of 2.36 V after 48 h, while the G and Celgard separators suffer fast voltage fading to 2.34 V and 2.25 V respectively, due to the severe self-discharge caused by the shuttle effect. In addition, favorable capacity retention of 989.7 mA h g<sup>-1</sup> and coulombic efficiency of 91.3% can be achieved by TiB2@G, which are much higher than those based on G (746.7 mA h g<sup>-1</sup> and 87.3%) and Celgard (426.9 mA h  $g^{-1}$  and 63.9%) separators. These results strongly manifest the superior self-discharge performance of TiB2@G, which reflects the admirable inhibition of polysulfide shuttling attributed to the structural superiorities of this separator design. Apart from that, highloading performance was also evaluated based on a raised areal sulfur loading of 4.5 mg cm<sup>-2</sup> in cathode. Fig. 5c shows the rate performance of high-loading electrode with TiB<sub>2</sub>@G separator. High areal capacity of  $5.8\,\text{mA}\,\text{h}\,\text{cm}^{-2}$  and  $2.8\,\text{mA}\,\text{h}\,\text{cm}^{-2}$  can be achieved at 0.05C and 1.0C, respectively, while the discharge curves well maintain the two-plateau profiles at varied current rate (Fig. 5c and d), indicating the good sulfur utilization and fast reaction kinetics even under a high-loading configuration benefiting from this separator design. Furthermore, the TiB<sub>2</sub>@G separator also enables a good cycling performance of the high-

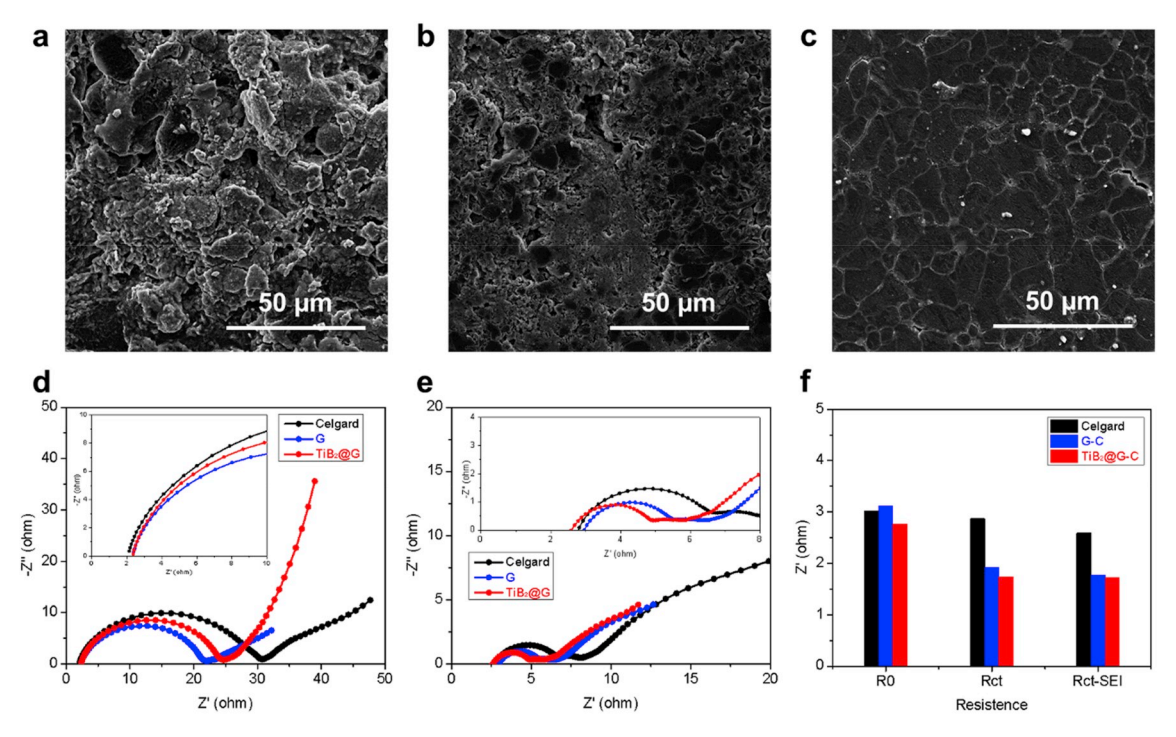


Fig. 4. FESEM images of surface of lithium foil after cycling of a. Celgard; b. G and c.  $TiB_2@G$ ; The EIS comparisons of Celgard, G and  $TiB_2@G$  d. before and e. after cycling. f. Impendences distribution comparisons of Celgard, G and  $TiB_2@G$  after cycling.

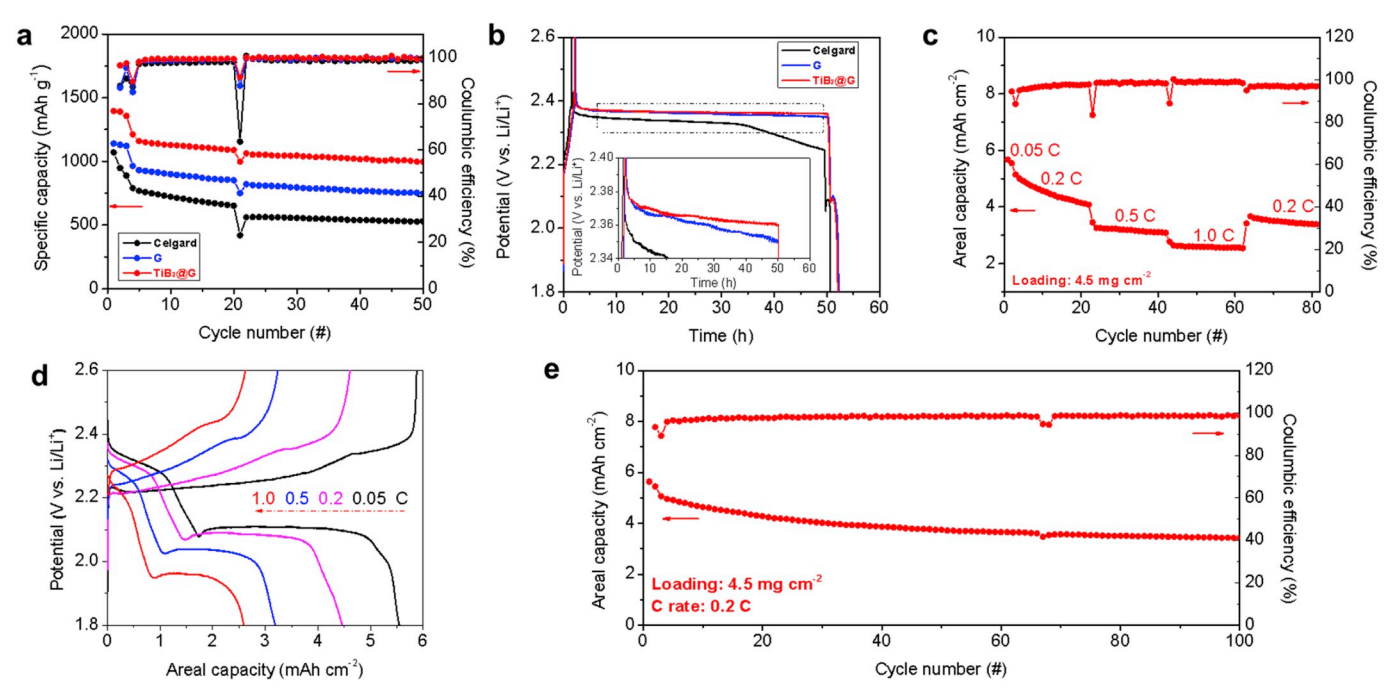


Fig. 5. a-b. Self-discharge evaluations of Celgard, G and  $TiB_2@G$ ; c. Multi-rate performance and d. profiles of  $TiB_2@G$  with the loading of 4.5 mg cm<sup>-2</sup>; e. Long-term cycling performance of  $TiB_2@G$  at 0.2C with the loading of 4.5 mg cm<sup>-2</sup>.

loading electrode with a decent capacity retention of 60% after 100 cycles at 0.2C. Some capacity drops during cycle are possibly ascribed to the test circumstance temperature change, which is recovered when the temperature returns to be normal. These results strongly manifest the great potential of the as-developed  $TiB_2@G$  separator for practical applications.

#### 4. Conclusion

In summary, we developed a metallically conductive  $TiB_2$  as multifunctional modifier to construct an advanced  $TiB_2@G$  separator for improved Li–S batteries. Coupled with two-dimensional graphene, the obtained  $TiB_2@G$  separator exhibit a synergistic combination of strong physical and chemical sulfur immobilizations as well as an efficient sulfur reutilization, thus establishing a reliable barrier toward inhibited shuttle effect and stabilized sulfur electrochemistry. As a result, cells

with  $TiB_2@G$  separator display a high capacity up to  $1350 \, \text{mA} \, \text{h g}^{-1}$  and outstanding cyclability with a capacity retention over 85% after 300 cycles at 0.5C. Meanwhile, the metallically conductive  $TiB_2$  promotes the sulfur reaction kinetic and enables a superb rate capability up to 5.0C. Beyond that, significantly mitigated self-charge behavior and admirable high-loading performance can be also achieved by the  $TiB_2@G$  separator design. This work offers a highly effective multifunctional separator for improved electrochemical performance, paving the way to future practical application of Li–S batteries.

## Acknowledgements

The authors acknowledge the financial support from the National Science Foundation of China, Grant Nos. 21776245, 21476200 and 511777140, the Science and Technology Commission of Shanghai Municipality (16DZ2290300, 17DZ1200403), and the Fundamental Research Funds for the Central Universities at Tongji University (22120180519/22120180308). And this work was also partly supported by National Science Foundation of the United States under Grant No. 1805288.

#### Appendix A. Supplementary data

Supplementary data to this article can be found online at https://doi.org/10.1016/j.jpowsour.2019.227336.

#### References

- [1] A. Manthiram, Y. Fu, S. Chung, C. Zu, Y. Su, Chem. Rev. 114 (2014) 11751–11787.
- [2] C. Shen, J. Xie, M. Zhang, P. Andrei, M. Hendrickson, E. Plichta, J. Zheng, Electrochim. Acta 248 (2017) 90–97.
- [3] C. Shen, J. Xie, M. Zhang, J. Zheng, M. Hendrickson, E. Plichta, J. Electrochem. Soc. 164 (2017) A1220–A1222.
- [4] G. Li, Z. Chen, J. Lu, Chem 4 (2018) 3-7.
- [5] G. Li, S. Wang, Y. Zhang, M. Li, Z. Chen, J. Lu, Adv. Mater. 30 (2018) 1705590.
- [6] L. Jin, F. He, W. Cai, J. Huang, B. Liu, Z. Li, J. Power Sources 328 (2016) 536–542.
- [7] C. Wang, W. Cai, G. Li, B. Liu, Z. Li, ChemElectroChem 5 (2018) 112-118.
- [8] G. Li, W. Lei, D. Luo, Y. Deng, D. Wang, Z. Chen, Adv. Energy Mater. 8 (2018) 1702381.
- [9] G. Li, W. Lei, D. Luo, Y. Deng, Z. Deng, D. Wang, A. Yu, Z. Chen, Energy Environ. Sci. 11 (2018) 2372–2381, 10.
- [10] W. Cai, G. Li, D. Luo, G. Xiao, S. Zhu, Y. Zhao, Z. Chen, Y. Zhu, Y. Qian, Adv. Energy Mater. 8 (2018) 1802561.
- [11] J. Ni, L. Jin, M. Xue, J. Zheng, J.P. Zheng, C. Zhang, Electrochim. Acta 296 (2019) 39–48.

- [12] I. Ousmane, R. Li, C. Wang, G. Li, W. Cai, B. Liu, Z. Li, Microporous Mesoporous Mater. 266 (2018) 276–282.
- [13] W. Cai, G. Li, K. Zhang, G. Xiao, C. Wang, K. Ye, Z. Chen, Y. Zhu, Y. Qian, Adv. Funct. Mater. 28 (2018) 1704865.
- [14] S. Zhang, Electrochim. Acta 70 (2012) 344-348.
- [15] W. Li, H. Yao, K. Yan, G. Zheng, Z. Liang, Y. Chiang, Y. Cui, Nat. Commun. 6 (2015) 7436.
- [16] L. Jin, G. Li, B. Liu, Z. Li, J. Zheng, J. Zheng, J. Power Sources 355 (2017) 147–153.
- [17] W. Cai, G. Li, F. He, L. Jin, B. Liu, Z. Li, J. Power Sources 283 (2015) 524-529.
- [18] Y. Su, A. Manthiram, Chem. Commun. 48 (2012) 8817-8819.
- [19] Y. Su, A. Manthiram, Nat. Commun. 3 (2012) 1166.
- [20] A. Rosenman, E. Markevich, G. Salitra, D. Aurbach, A. Garsuch, F. Chesneau, Adv. Energy Mater. 5 (2015) 1500212.
- [21] H. Peng, J. Huang, X. Cheng, Q. Zhang, Adv. Energy Mater. 7 (2017) 1700260.
- [22] Y. Hu, W. Chen, T. Lei, B. Zhou, Y. Jiao, Y. Yan, X. Du, J. Huang, C. Wu, X. Wang, Y. Wang, B. Chen, J. Xu, C. Wang, J. Xiong, Adv. Energy Mater. 9 (2019) 1802955.
- [23] Y. Pang, J. Wei, Y. Wang, Y. Xia, Adv. Energy Mater. 8 (2018) 1702288.
- [24] H. Kim, J. Hwang, A. Manthiram, Y. Sun, ACS Appl. Mater. Interfaces 8 (2016)
- [25] G. Ma, Z. Wen, Q. Wang, C. Shen, P. Peng, J. Jin, X. Wu, J. Power Sources 273 (2015) 511–516.
- [26] X. Wang, Z. Wang, L. Chen, J. Power Sources 242 (2013) 65-69.
- [27] J. Huang, Z. Xu, S. Abouali, M. Akbari Garakani, J. Kim, Carbon 99 (2016) 624–632.
- [28] J. Balach, T. Jaumann, M. Klose, S. Oswald, J. Eckert, L. Giebeler, J. Phys. Chem. C 119 (2015) 4580–4587.
- [29] J. Sun, Y. Sun, M. Pasta, G. Zhou, Y. Li, W. Liu, F. Xiong, Y. Cui, Adv. Mater. 28 (2016) 9797–9803.
- [30] Z. Ghazi, X. He, A. Khattak, N. Khan, B. Liang, A. Iqbal, J. Wang, H. Sin, L. Li, Z. Tang, Adv. Mater. 29 (2017) 1606817.
- [31] T. Zhou, W. Lv, J. Li, G. Zhou, Y. Zhao, S. Fan, B. Liu, B. Li, F. Kang, Q. Yang, Energy Environ. Sci. 7 (2017) 1694–1703.
- [32] X. Yue, X. Li, J. Meng, X. Wu, Y. Zhou, J. Power Sources 397 (2018) 150-156.
- [33] Y. Lai, P. Wang, F. Qin, M. Xu, J. Li, K. Zhang, Z. Zhang, Energy Storage Mater. 9 (2017) 179–187.
- [34] X. Tao, J. Wang, C. Liu, H. Wang, H. Yao, G. Zheng, C. Zu, Nat. Commun. 7 (2016) 11203.
- [35] Wang, M. Feng, H. Sun, G. Li, Q. Fu, H. Li, J. Liu, L. Sun, A. Mauger, C.M. Julien, H. Xie, Z. Chen, Nano Energy 59 (2019) 390–398.
- [36] C. Li, X. Liu, L. Zhu, R. Huang, M. Zhao, L. Xu, Y. Qian, Chem. Mater. 30 (2018) 6969–6977.
- [37] N.J. Welham, J. Am. Ceram. Soc. 83 (2004) 1290-1292.
- [38] Q. Pang, C.Y. Kwok, D. Kundu, X. Liang, L.F. Nazar, Joule 3 (2019) 136-148.
- [39] L. Jin, R. Gong, J. Zheng, C. Zhang, Y. Xia, J. Zheng, ChemElectroChem 6 (12) (2019) 3020–3029.
- [40] L. Jin, J. Zheng, Q. Wu, A. Shellikeri, S. Yturriaga, R. Gong, J. Huang, J.P. Zheng, Mater. Today Energy 7 (2018) 51–57.
- [41] L. Jin, R. Gong, W. Zhang, Y. Xiang, J. Zheng, Z. Xiang, C. Zhang, Y. Xia, J. P. Zheng, J. Mater. Chem. A 7 (2019) 8234–8244.
- [42] L. Jin, X. Guo, R. Gong, J. Zheng, Z. Xiang, C. Zhang and J. P. Zheng, Energy Storage Mater., DOI:10.1016/j.ensm.2019.04.027.